

Downscaled rainfall projections in south Florida using self-organizing maps

Palash Sinha ^a, Michael E. Mann ^a, Jose D. Fuentes ^{a,*}, Alfonso Mejia ^a, Liang Ning ^b, Weiyi Sun ^b, Tao He ^b, Jayantha Obeysekera ^c

^a The Pennsylvania State University, University Park, PA, USA

^b School of Geography Science, Nanjing Normal University, Nanjing, China

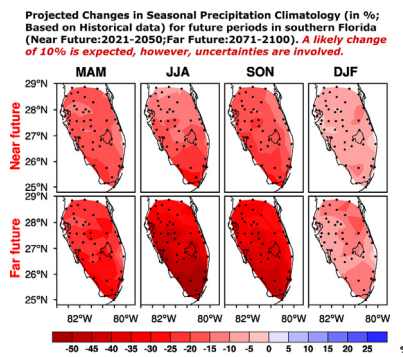
^c South Florida Water Management District, West Palm Beach, FL, USA.



HIGHLIGHTS

- Downscaling of rainfall totals in south Florida, U.S., reproduced observed values during the historical period (1976–2005).
- Raw climate model outputs poorly replicated historical rainfall totals but statistical downscaling reproduced observed values.
- Projections of future rainfall yielded drying conditions, magnitude depends on timeframe and future greenhouse gas emissions.
- Anticipated frequency of wet days will likely decrease and the average length of dry spells increases.

GRAPHICAL ABSTRACT



ARTICLE INFO

Article history:

Received 22 July 2017

Received in revised form 26 February 2018

Accepted 9 April 2018

Available online xxxx

Keywords:

Climate
Rainfall
Drought
Downscaling
Hydrology

ABSTRACT

We make future projections of seasonal precipitation characteristics in southern Florida using a statistical downscaling approach based on Self Organized Maps. Our approach is applied separately to each three-month season: September–November; December–February; March–May; and June–August. We make use of 19 different simulations from the Coupled Model Inter-comparison Project, phase 5 (CMIP5) and generate an ensemble of 1500 independent daily precipitation surrogates for each model simulation, yielding a grand ensemble of 28,500 total realizations for each season. The center and moments (25thile and 75thile) of this distribution are used to characterize most likely scenarios and their associated uncertainties. This approach is applied to 30-year windows of daily mean precipitation for both the CMIP5 historical simulations (1976–2005) and the CMIP5 future (RCP 4.5) projections. For the latter case, we examine both the “near future” (2021–2050) and “far future” (2071–2100) periods for three scenarios (RCP2.6, RCP4.5, and RCP8.5).

© 2018 Elsevier B.V. All rights reserved.

1. Introduction

Key climate change impacts are found at regional and local scales. Several studies (Hartmann et al., 2013; Portmann et al., 2009) demonstrate that climate change has so far had substantial impacts on the hydrological cycle and associated extreme weather events. With the

* Corresponding author.

E-mail address: jdfuentes@psu.edu (J.D. Fuentes).

advancement of computer resources and more accurate representations of large-scale atmospheric processes, General Circulation Models (GCMs) are able to represent changes in temperature and precipitation (Sarojini et al., 2012; Kumar et al., 2013) at large-scales. However, present-day GCMs are typically run at fairly coarse spatial resolution (average latitudinal resolution is 1.3°, Taylor et al., 2011), such that key physical processes (such as regional convection) may not be well resolved. The direct (what we refer to as “raw”) output from GCMs may thus not provide reliable or useful information about regional and local changes in climate, including hydroclimatic phenomena at local (<100 km) spatial and short (daily) temporal scales. Given the importance of such information for key stakeholders and policymakers, alternative means for assessing local hydroclimatic impacts of climate are needed (Wagener et al., 2010).

One approach to solving this problem involves the use of downscaling techniques to produce finer or local scale weather and climate information (Wood et al., 2004). These techniques can be broadly divided into statistical and dynamical downscaling (Wilby and Wigley, 1997; Murphy, 1999). Statistical downscaling techniques seek relationships between local scale variables (referred as predictant variables) and characteristics of large-scale fields (referred as predictor variables) (Hewitson and Crane, 1992; Wilks, 1995; Hewitson and Crane, 1996; Ning et al., 2012a). In the Fourth Assessment Report of the Intergovernmental Panel on Climate Change (IPCC, AR4), the performance of several downscaling techniques was assessed (Christensen et al., 2007), establishing that downscaling techniques can improve the GCM-based climate simulation at the local scale. The IPCC AR5 assessment (2013) further demonstrated the utility of downscaling techniques for improved local-scale information climate assessments (Flato et al., 2013). Although several downscaling methods have been used (Cavazos, 1997; Crane and Hewitson, 1998; Wilby et al., 1998; Crane et al., 2002), statistical approaches using artificial neural networks (ANNs) are increasingly favored due to their capacity for capturing nonlinear relationships between predictors and predictants (Snell et al., 2000; Schoof and Pryor, 2001; Hewitson and Crane, 2006; Ning et al., 2012a).

Previous studies (Trimble et al., 2005; Obeysekerera et al., 2011; Goly and Teegavarapu, 2013; Swain et al., 2014) used the GCMs and downscaled GCMs outputs to investigate the characteristics of precipitation over the Florida region, U.S. Trimble et al. (2005) examined the usefulness of teleconnections between south Florida rainfall and natural climate variability for the purpose of water management strategies in that region. Obeysekerera et al. (2011) extensively investigated the performance of several GCMs of Coupled Model Inter-comparison Project, phase 3 (CMIP3) for Florida, and concluded that GCMs have limited skill in representing the local-scale characteristics of temperature and precipitation. They also illustrated that direct outputs of GCMs may not be sufficiently “reliable” for water management policies. In particular, the projections of precipitation are difficult because most GCMs poorly present regional and small-scale convection and phenomena such as breezes due to the coarse resolutions of models (Murphy, 1999; Wilby et al., 1998; Schoof et al., 2009). Goly and Teegavarapu (2013) examined statistical techniques such as positive coefficient regression and multiple linear regression and Goyal and Ojha (2010) applied stepwise regression and bias correction spatial disaggregation (BCSD), and for precipitation downscaling from GCMs to single stations in Florida. In addition, Tripathi et al. (2006) used support vector machine (a kernel based neural network) and Sinha et al. (2013) employed canonical correlation techniques, to derive statistical downscaling of precipitation at monthly and seasonal time scales in India. Such studies revealed that the downscaled precipitation is closer to observations as compared to GCM outputs. Their studies also indicate that support vector machine performs better than other techniques. Other studies (Khan et al., 2006; Rousi et al., 2015) indicate that the performances of ANN-based downscaling approaches are reliable and satisfactory; however, the same is yet to be evaluated for the Florida region.

Crane and Hewitson (1998) applied ANN-based approaches for downscaling precipitation over mid-Atlantic and northeast regions of the U.S., and found significant amount of changes in precipitation during spring and summer. The Self-Organizing Maps (SOM) (Kohonen, 1989) based downscaling methodology (Hewitson and Crane, 2006) was evaluated on precipitation downscaling at the station level in Pennsylvania, U.S. by Ning et al. (2012a). They used predictor fields from CMIP3 model outputs to downscale precipitation over seventeen stations in Pennsylvania. They demonstrated that characteristics (intensity and variability) of precipitation in the downscaled output agree more closely to observations than the ones generated from raw GCM outputs. The SOM is a two-dimensional array of nodes, where a vector representing the average of the surrounding points in the original data space describes each node. A matrix of ‘n’ variable data points and ‘m’ observations represent the input dataset. In the SOM, a reference vector of length n describes each node. The initial step in the SOM training involves assigning random values to each node reference vector and then comparing the data record with each node vector. The reference vector that most closely matches the data vector is defined as the ‘winning’ node. Then, the reference vector of the winning node is updated slightly towards the direction of the input data by a factor termed the ‘learning rate’. All the surrounding nodes are also updated in the direction of the input data by a smaller learning rate. The entire process is then repeated for multiple iterations until the differences between iterations are smaller than a selected threshold value. Crane and Hewitson (2003) described this training procedure.

It is important to recognize that the SOM and the BCSD belong to different categories of downscaling methods (Maraun et al., 2010). The SOM-based downscaling belongs to the ‘perfect prognosis’, which builds statistical relationships between atmospheric synoptic circulation patterns and regional variables (precipitation and temperature) and applies the resulting relationships to the model simulated synoptic circulation patterns. In contrast, the BCSD belongs to model output statistics, which directly applies to the statistical processing methods to the model simulated precipitation and temperature data. Therefore, it is expected that the results from the SOM-based downscaling and BCSD may yield different results.

The IPCC Fifth Assessment Report (AR5) shows that, during the period 1951–2010, over the Florida region, trends in precipitation are positive (greater precipitation) with the use of Global Historical Climatology Network (GHCN) data while the computed trend is negative when Global Precipitation Climatology Centre (GPCC) data are used (Hartmann et al., 2013). On the other hand, instrumental records from the Climate Research Unit (CRU) indicate positive trends over northern parts of Florida and negative trends over southern parts of Florida. Furthermore, the IPCC AR5 (Flato et al., 2013) indicates that the probability of the decrease in precipitation will be higher over the region in the projected future climate scenarios. However, characteristics of precipitation may vary from region to region over the southeastern parts of North America. The GCMs are not capable to depict the spatial variations of meteorological variables, especially precipitation at fine scale (Obeysekerera et al., 2011). Thus, for improved understanding of climate changes at local scales, the GCMs outputs are needed to translate into high resolution. To generate hydroclimatic projections, hydrological models normally require high-resolution climate change data from downscaling methods. This means that climate information must be provided at comparable spatial resolution to adequately investigate changes in hydrological variables (Krause et al., 2005). Wood et al. (2004) applied the BCSD method to both Parallel Climate Model (PCM) and Regional Climate Model (RCM) outputs and revealed that the BCSD method could reproduce the key characteristics of observed hydrometeorological conditions in both cases.

South Florida is the peninsular region of North America, and its current population is approximately 6 million and is expected to reach around 15 million in the next 30 years (Rayer and Wang, 2017). With the increase in population, the need for water will

grow by 2.5 times to maintain a sustainable societal demand (Smith and Rayer, 2013). As a consequence of global warming and sea level rise, the quantity and the quality of water for drinking and low-lying agricultural and forested areas will be perniciously impacted. In the context of climate change scenarios, precipitation patterns and intensity can be modulated in the future (Portmann et al., 2009). Information about the anticipated changes in rainfall patterns at local scale are required to develop sustainable water use policy and decision-making on adaptation strategies. Therefore, in

this study, our goal is to evaluate the appropriateness and the advantages of ANN-based approaches (Hewitson and Crane, 2006) for the downscaling of rainfall estimates in south Florida. We select ANN-based approaches because of their improved performance over other statistical downscaling methods. For the regional downscaling, the Coupled Model Inter-comparison Project, phase 5 (CMIP5) model outputs are employed as predictor variables to determine the daily rainfall at the station level. Using the downscaled outputs, the projected changes in precipitation over south Florida

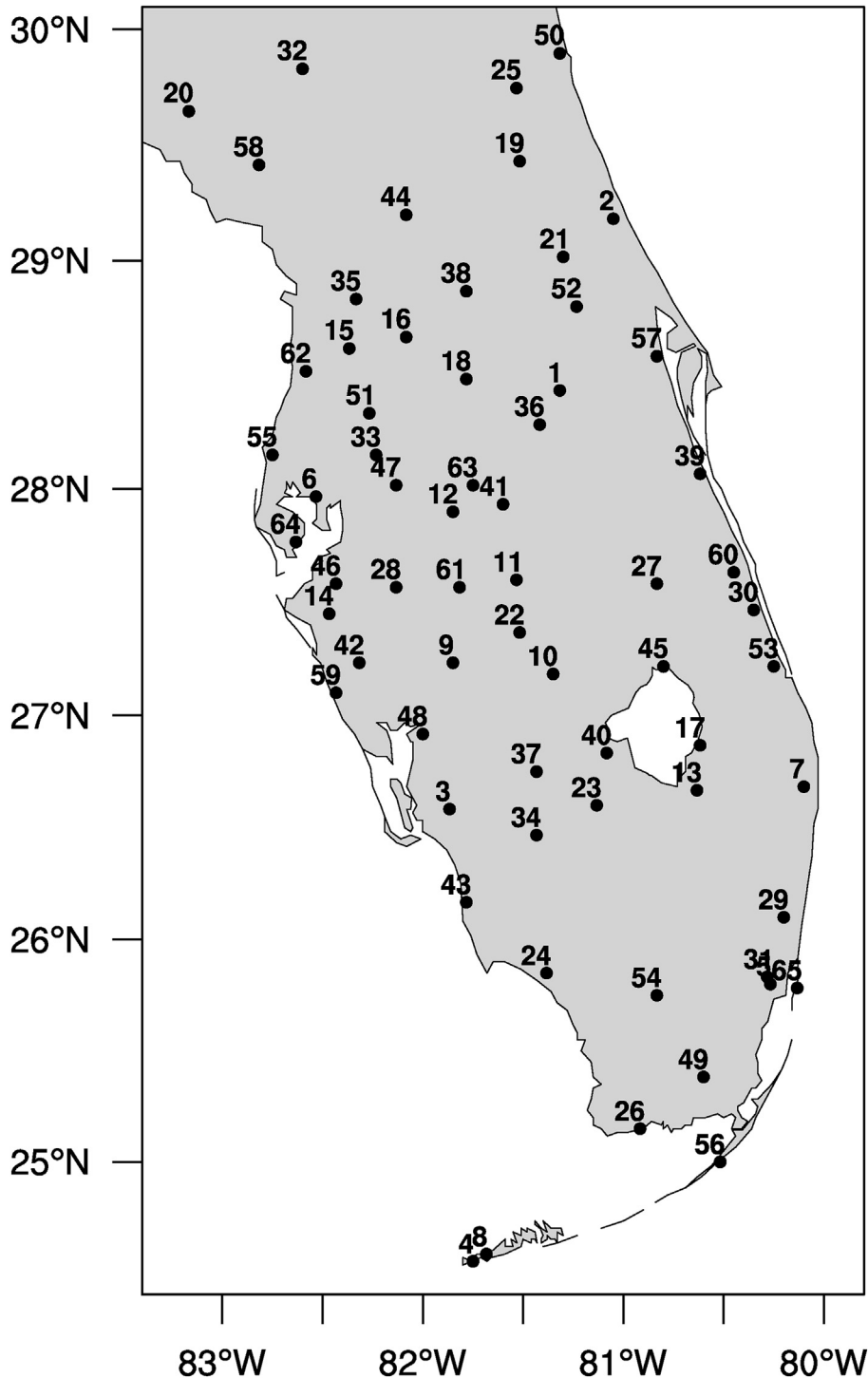


Fig. 1. Locations of the observation stations (65 stations) in south Florida included in this study. Station names and corresponding latitude-longitude locations (according to serial numbers) are provided in Table 1.

for the “near future” (2021–2050) and “far future” (2071–2100) periods are examined. Prior to that, the uncertainties associated with the employed approaches, for the period of the instrumental record (1976–2005), are determined and assessed.

2. Data and methodology

2.1. Study region

This study includes the Florida region that is bounded from 25°N to 30°N in the north–south and from 87°W to 80°W in the east–west direction (Fig. 1). The study area is the peninsular region of Florida and is situated between the Gulf of Mexico and the Atlantic Ocean. This region has flat and low-lying terrain having elevation less than (or equal to) 3.7 m. However, the average elevation for the state of Florida is approximately 30 m from mean sea level (Kosovich, 2008). The Everglades covers (with an area of approximately 13,000 km²) a large part of the southern half of south Florida and is a subtropical marshy land, swampy, and a partly forested region. This region is characterized by clumps of tall sawgrass and slough systems. It has well defined wet and dry seasons. The wet season spans from June to October and the dry season includes November to May. In general, the hottest periods span from mid-May to mid-October. The peak rainy season extends from June to August (hereafter referred to as JJA) while peak boreal winter is from December to February (hereafter referred to as DJF). The region is characterized by extreme weather events such as heavy rainfall caused by tropical storms, and droughts that have impacts on water supplies and agriculture. Sea level is changing at the rate of 1–3 mm per year (Rhein et al., 2013) and the rate of inflow of salty water is also increasing through coastal areas. The incursion of salty water affects the highly valued agricultural systems in south Florida (Harrington and Walton, 2007).

2.2. Data

In this study, we use three sets of data for the downscaling procedure: National Centers for Environmental Prediction (NCEP) reanalysis of daily gridded atmospheric data, observed daily station precipitation data, and GCM daily gridded atmospheric data. Daily mean precipitation observations over 65 stations in the Florida region were obtained from the National Oceanic and Atmospheric Administration (NOAA)'s National Climate Data Center (NCDC) (<http://www.ncdc.noaa.gov/cdo-web/>). Fig. 1 shows the geographical location of the stations and Table 1 provides associated latitude–longitude information and name of the station. Atmospheric variables from the NCEP–National Center for Atmospheric Research (NCAR) reanalysis gridded data (Kalnay et al., 1996) and General Circulation Model's (GCM's) outputs from the Climate Model Inter-comparison Project (CMIP, phase 5; CMIP5) outputs (Taylor et al., 2011) were used: zonal and meridional components of the wind speed at the 10-m height and 700-hPa pressure level, relative humidity at the 850-hPa pressure level, air temperature anomalies at the 2-m height, and temperature lapse rate between 850 and 500-hPa pressure levels. These meteorological variables were selected because of their dominance on occurrences of local precipitation.

The GCM daily frequency gridded data are available from the Program for Climate Model Diagnosis and Inter-comparison (PCMDI; <http://pcmdi9.llnl.gov/esgf-web-fe/live#>). In the historical simulations of CMIP5 models, changes of several important atmospheric and land surface conditions (e.g., solar forcing, concentrations of aerosols from both natural and anthropogenic sources, atmospheric composition due to anthropogenic and volcanic influences, and land use) are consistent with the observations during the historical era (Taylor et al., 2011). For future simulations of CMIP5 models, we consider three different representative greenhouse concentration pathways (RCP), namely RCP2.6, RCP4.5, and RCP8.5 scenarios. These scenarios are based on impacts of different scales of greenhouse gas emissions. For example, the

Table 1

Stations names and locations (according to serial numbers shown in Fig. 1) considered for the present study.

Sl no.	Station name	Latitude	Longitude	Sl no.	Station name	Latitude	Longitude
1	Orlando	28.433	−81.317	34	Immokalee	26.467	−81.433
2	Daytona beach Int. Air.	29.183	−81.05	35	Inverness 3 SE	28.833	−82.333
3	Fort Myers page field	26.583	−81.867	36	Kissimmee 2	28.283	−81.417
4	Key West Inter. Airport	24.55	−81.75	37	La Belle	26.75	−81.433
5	Miami Inter. Airport	25.8	−80.267	38	Lisbon	28.867	−81.783
6	Tampa Intern. Airport	27.967	−82.533	39	Melbourne	28.067	−80.617
7	West Palm Beach	26.683	−80.1	40	Moore Haven	26.833	−81.083
8	Key West	24.583	−81.683	41	Mountain Lake	27.933	−81.6
9	Arcadia	27.233	−81.85	42	Myakka	27.233	−82.317
10	ArchboldBio Station	27.183	−81.35	43	Naples	26.167	−81.783
11	Avon Park	27.6	−81.533	44	Ocala	29.2	−82.083
12	Bartow	27.9	−81.85	45	Okeechobee	27.217	−80.8
13	Belle Glade	26.667	−80.633	46	Parrish	27.583	−82.433
14	Bradenton	27.45	−82.467	47	Plant City	28.017	−82.133
15	Brooksville	28.617	−82.367	48	Punta Gorda	26.917	−82
16	Bushnell	28.667	−82.083	49	Royal Palm	25.383	−80.6
17	Canal Point	26.867	−80.617	50	St Augustine	29.9	−81.317
18	Clermont	28.483	−81.783	51	Saint Leo	28.333	−82.267
19	Crescent City	29.433	−81.517	52	Sanford	28.8	−81.233
20	Cross City	29.65	−83.167	53	Stuart	27.217	−80.25
21	Deland	29.017	−81.3	54	Tamiami	25.75	−80.833
22	Desoto City	27.367	−81.517	55	Tarpon	28.15	−82.75
23	Devils garden	26.6	−81.133	56	Tavernier	25	−80.517
24	Everglades	25.85	−81.383	57	Titusville	28.583	−80.833
25	Federal Point	29.75	−81.533	58	Usher Tower	29.417	−82.817
26	Flamingo Ranger Stn	25.15	−80.917	59	Venice	27.1	−82.433
27	Fort Drum	27.583	−80.833	60	Vero Beach	27.633	−80.45
28	Fort Green	27.567	−82.133	61	Wauchula	27.567	−81.817
29	Fort Lauderdale	26.1	−80.2	62	WeekiWachee	28.517	−82.583
30	Fort Pierce	27.467	−80.35	63	Winter Haven	28.017	−81.75
31	Hialeah	25.833	−80.283	64	St Petersburg Albert	27.767	−82.633
32	High Springs	29.833	−82.6	65	Miami Beach	25.783	−80.133
33	Hillsborough River State	28.15	−82.233				

RCP4.5 scenario is the central scenario in which the radiative forcing will reach 4.5 W m^{-2} by 2100 and stabilize afterwards (Clarke et al., 2007a, 2007b). The RCP2.6 and RCP8.5 scenarios are considered to understand the minimum and extreme impact of greenhouse gases in the projected precipitation. Also, the central scenario represents the most likely climate state of the projected future (Moss et al., 2010; Taylor et al., 2011). Here, we employ nineteen GCM models from the CMIP5 (http://cmip-pcmdi.llnl.gov/cmip5/data_portal.html) and provide the relevant model information in Table 2.

We consider three data sets for “historical” (from January 1, 1976 to December 31, 2005), “near future” (January 1, 2021 to December 31, 2050), and “far future” (January 1, 2071 to December 31, 2100) periods for precipitation downscaling. Each of the periods consists of 30 years. For the GCM data sets, long-term historical simulations are considered for the past period and all the three scenarios for future periods.

2.3. Regional downscaling methodology

2.3.1. The SOM procedure

Before applying the downscaling procedure, we converted all GCMs and NCEP-NCAR reanalysis data into the regular grid size of $2.0^\circ \times 2.0^\circ$ to keep atmospheric variables in the same horizontal resolution (222 km). The present downscaling technique is based on the previously applied SOM approach (Hewitson and Crane, 2006). The SOM method uses the synoptic features of the meteorological variables surrounded by the location/point to determine the characteristic modes for downscaling. This method is based on the fuzzy-clustering

algorithm and widely used to visualize and characterize multivariate data sets (Kohonen, 1989, 1995). It identifies the groups of input variables with certain common characteristics and enables to reduce large and multi-dimensional data sets into fewer dimensions. A ‘Kohonen’ SOM consists of nodes of two-dimensional arrays, and each node is represented by a feature vector having the same length as the number of input variables. The input variables are fully connected with the output in the SOM approach. The weights of the connections between the nodes and the input variables are described as components of the feature vector. In the “training” of a SOM, initially random small values are given as weights and compare each node (feature) with the data vectors and the closest node vector is considered as “winning” node. Then the winning vector is updated by a process known as the “learning” (and with a rate termed as “learning rate”) to modify the vector towards the input data direction. In this process, the neighboring nodes are also modified towards input data direction by a smaller learning rate. As this process is repeated, the node vectors are gradually modified, and neighboring nodes have the similar feature vectors. The Euclidean distance to all node vectors defines the similarity between the vectors. This process is continued until the measured distance reaches a selected threshold value.

In the present study, we use the seven variables obtained from NCEP-NCAR reanalysis to generate the SOM (Fig. 2). Firstly, one particular node that is closest to the observed daily atmospheric data is selected for each day. Then we consider all those days that are mapped onto that particular node and rank the precipitation of those days from low to high. In order to define a continuous cumulative

Table 2
CMIP5 coupled models with their names and horizontal resolutions (longitude \times latitude, in degrees) considered for this study. A single realization i.e., realization r1i1p1 is used for all models.

Sl. no.	Model Acronym	Expansion	Institute, Country	Atmospheric resolution (Lon \times Lat)
1*	ACCESS1-0	Australian Community Climate and Earth System Simulator coupled model	Centre for Australian Weather and Climate Research (CAWCR), Australia	$1.9^\circ \times 1.25^\circ$
2*	ACCESS1-3	Australian Community Climate and Earth System Simulator coupled model	CAWCR, Australia	$1.9^\circ \times 1.25^\circ$
3*	CMCC-CM	Centro Euro-Mediterraneo sui Cambiamenti Climatici (CMCC) Climate Model	Centro Euro-Mediterraneo sui Cambiamenti Climatici (CMCC), Italy	$0.8^\circ \times 0.8^\circ$
4*	CMCC-CMS	CMCC Coupled Modelling System	CMCC, Italy	$1.9^\circ \times 1.9^\circ$
5*	CNRM-CM5	Centre National de Recherches Météorologiques Coupled Global Climate Model, version 5	Centre National de Recherches Météorologiques (CNRM)/Centre Européen de Recherche et de Formation Avancée en Calcul Scientifique (CERFACS), France	$1.4^\circ \times 1.4^\circ$
6*	MIROC-ESM	Model for Interdisciplinary Research on Climate (MIROC), Earth System Model	Atmosphere and Ocean Research Institute (AORI), The University of Tokyo, National Institute for Environmental Studies (NIES), and Japan Agency for Marine-Earth Science and Technology (JAMSTEC), Japan	$2.8^\circ \times 2.8^\circ$
7*	MIROC-ESM-CHEM	MIROC Earth System Model	AORI (The University of Tokyo), NIES, and JAMSTEC, Japan	$2.8^\circ \times 2.8^\circ$
8*	MPI-ESM-LR	Max Planck Institute (MPI) Earth System Model, low resolution	Max Planck Institute for Meteorology (MPI-M), Germany	$1.9^\circ \times 1.9^\circ$
9*	MPI-ESM-MR	MPI Earth System Model, medium resolution	MPI-M, Germany	$1.9^\circ \times 1.9^\circ$
10*	MRI-CGCM3	Meteorological Research Institute Coupled Atmosphere–Ocean General Circulation Model, version 3	Meteorological Research Institute (MRI), Japan	$1.1^\circ \times 1.1^\circ$
11**	BNU-ESM	Beijing Normal University Earth System Model	Beijing Normal University, China	$2.8^\circ \times 2.8^\circ$
12**	CanESM2	Second Generation Canadian Earth System Model	Canadian Centre for Climate Modelling and Analysis (CCCma), Canada	$2.8^\circ \times 2.8^\circ$
13**	GFDL-ESM2G	Geophysical Fluid Dynamics Laboratory (GFDL) Earth System Model (ESM) with Generalized Ocean Layer Dynamics (GOLD) component (ESM2G)	National Oceanic and Atmospheric Administration (NOAA)/Geophysical Fluid Dynamics Laboratory (GFDL), USA	$2.5^\circ \times 2.0^\circ$
14**	GFDL-ESM2M	GFDL-ESM with Modular Ocean Model 4 (MOM4) component (ESM2M)	NOAA/GFDL, USA	$2.5^\circ \times 2.0^\circ$
15**	IPSL-CM5A-LR	L’Institut Pierre-Simon Laplace Coupled Model (LMDZ4), version 5, coupled with NEMO, low resolution	L’Institut Pierre-Simon Laplace (IPSL), France	$3.75^\circ \times 1.9^\circ$
16**	IPSL-CM5A-MR	L’Institut Pierre-Simon Laplace (IPSL) Coupled Model, version 5, coupled with NEMO, medium resolution	IPSL, France	$2.5^\circ \times 1.2^\circ$
17**	IPSL-CM5B-LR	IPSL Coupled Model (LMDZ5), version 3.1, coupled with NEMO, low resolution	IPSL, France	$3.75^\circ \times 1.9^\circ$
18**	bcc-csm1-1	Beijing Climate Center Climate System Model, version 1.1 (bcc-csm1-1)	Beijing Climate Center (BCC), China	$2.8^\circ \times 2.8^\circ$
19**	bcc-csm1-1-m	bcc-csm1-1 with moderate resolution	BCC, China	$1.125^\circ \times 1.125^\circ$

Single asterisk represents that models consider the standard Gregorian calendar, i.e. they do consider 366 days for leap year. Double asterisk represents that models consider 365 days for each year, i.e., they do not consider 366 days for leap year.

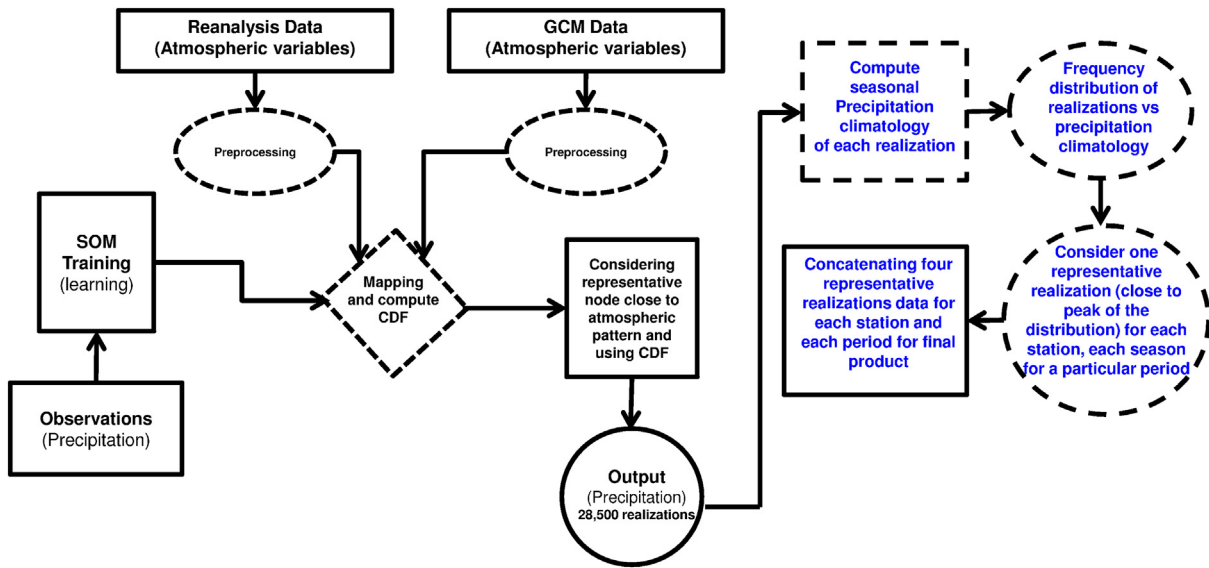


Fig. 2. Schematic diagram of the present downscaling process using self-organizing maps (SOMs). In the diagram, text in black color represents the SOM downscaling process and text in blue color represents the process to construct one prediction from SOM generated outputs (grand ensemble). (For interpretation of the references to color in this figure legend, the reader is referred to the web version of this article.)

distribution function (CDF) of the precipitation, a spline is fit to the ranked precipitation data of each node. This procedure is repeated for all the SOM nodes and all points. For each day, the atmospheric state of the GCMs data is closest to a particular node of the SOM. Then, the precipitation for that day is selected from the CDF of that node by using a random number generator. Ning et al. (2012a) provided a detailed description on the procedure to downscale GCM data using the SOM approach (Fig. 2).

For each station, the present SOM method generates 1500 sets of daily precipitation estimates using atmospheric information from one of the 19 GCMs. Each set can be referred to as a realization/ensemble member. Thus, we have 28,500 (1500 sets × 19 numerical models) realizations that represent the characteristics of daily precipitation for each period and each station. Realizations can be treated as a grand ensemble (i.e., 28,500 realizations).

2.3.2. Methodology to construct one-time daily precipitation from grand ensemble for each period and station

Usually, the ensemble average performs better than any single model simulation in reproducing observations. Previous studies (Brekke et al., 2008; Ning et al., 2012b) used different techniques to construct a single precipitation time series. The multi-model ensemble weighted-average technique is one of the useful methods; where, a weighted fraction of a model is the highest (lowest) in the future prediction if the performance of that model is the highest (lowest) in simulating the past climate. Therefore, according to Ning et al. (2012b), the model with higher skills in reproducing past climate will dominate the projected changes in the future. In this study, a single time series is constructed from the multi-model grand ensemble based on the frequency distribution of realizations and seasonal precipitation climatology for each station and period.

For each time period, we give equal weight to all the simulated precipitations obtained from SOM downscaling approach using different GCMs. In the procedure to generate one precipitation time series from the grand ensemble for each station, we first consider four different seasons, representing spring (MAM), summer (JJA), autumn (SON), and winter (DJF) and compute seasonal precipitation climatology using each realization data for a particular period. For a particular season, we estimate the frequency distribution of the 28,500 realizations in representing the precipitation climatology. We then consider one realization that represents or is close to the highest probability of the rainfall

distribution for that season. The same is repeated to find one best-fit realization for each season. The representative realizations for the four seasons may vary from station to station and from season to season. Thus, for a particular year, each station daily precipitation is represented by concatenating four representative realizations and continuing the process to estimate daily time series of precipitation for a particular period (Fig. 2).

As an example, consider one station (say S_1) for which daily precipitation time series is generated for the historical period. The seasonal precipitation climatology (mm per day) can be estimated by

$$\bar{P}_k = \left[\frac{1}{N_1} \sum_{i=1}^{N_1} \left\{ \frac{1}{N_2} \sum_{j=1}^{N_2} rf_{ij} \right\} \right] k \tag{1}$$

where \bar{P}_k represents the precipitation climatology for a particular season, k represents the number of realizations (here k runs from 1 to 28,500), N_1 is the number of years for the historical period (here 30 years), N_2 is the number of days of that season, and rf represents daily precipitation (mm) values obtained from the realization k . Thus, for the historical period and for a particular season, we have 28,500 values of seasonal precipitation climatology obtained from each realization. We then consider different categories of precipitation climatology with interval of 0.1 mm per days, starting from 0 mm per day. We estimate the distribution of the frequency of realization for precipitation climatology of different categories by

$$v_q = \frac{1}{N} (n_q) \tag{2}$$

where N is the total number of realizations (here 28,500), n_q is the number of realizations that simulate the precipitation climatology (precipitation climatology of a season can be represented by rain rate (mm per day) or total amount (mm) of precipitation for that season) in category q and v is the frequency of realization. A typical example for the frequency distribution of realization and seasonal precipitation climatology is shown in Fig. 3. Next, we choose the realization that is close to the peak of the frequency distribution and consider it as the representative realization for that season. In a similar fashion, we select one realization for each season (DJF, MAM, and JJA) separately. Therefore, for the historical period, four realizations represent four seasons at a

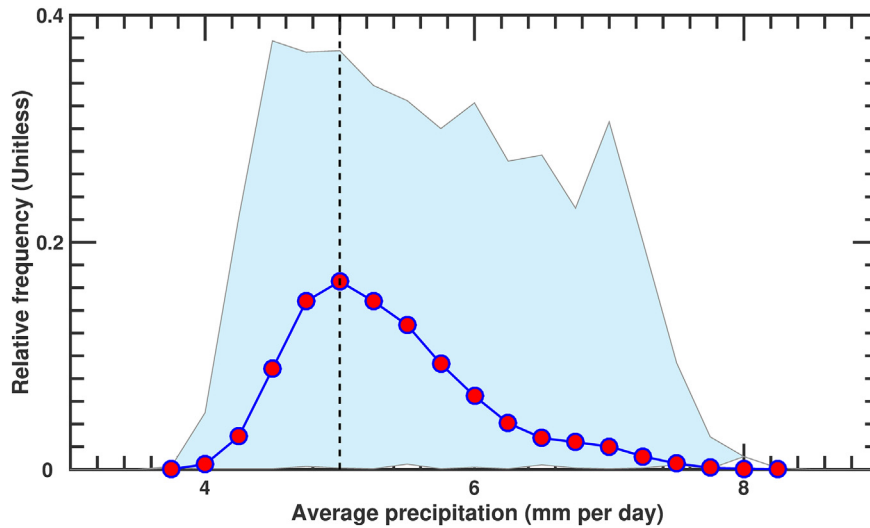


Fig. 3. Frequency distribution of seasonal mean rainfall (in mm per day; for the SON season) for the Miami International Airport station during the historical period of 1976–2005 (the red circles denote the grand ensemble mean while the shaded region indicates the spread among realizations in the grand ensemble). (For interpretation of the references to color in this figure legend, the reader is referred to the web version of this article.)

particular station. We construct one single time series using four representative realizations by concatenating successively the daily precipitation data of representative realizations for DJF, MAM, JJA, and SON. Finally, we merge all year's data and construct onetime series for station S_1 in the historical period. The above procedure is repeated for all stations and separately for each period. A different approach is employed to generate a precipitation time series from the grand ensemble. In this approach, we consider the representative realization that simulates the precipitation climatology close to the observations and the same representative realization is used for historical and future periods. Both approaches show almost similar signals in the projected precipitation patterns. Therefore, we only present the results obtained from the first method.

3. Results and discussion

Here we evaluate the performance of the climate downscaling in order to summarize and discuss the results from applying the proposed downscaling method including comparison of downscaled and observed precipitation and validation of the downscaled products.

3.1. Training of SOM with NCEP reanalysis data

The NCEP reanalysis of meteorological data is used to train the SOM. Also, the SOM is employed to generate daily rainfall sequences during the 1976 to 2005 training interval to access the performance of the downscaling method. We generate 1500 realizations using the downscaling procedure. The probability distribution method described earlier (Section 2.3.2) is employed to select a single representative time series.

In south Florida, there are distinct dry and wet seasons. During the spring onset of the rainy season (MAM), total rainfall in such a period can reach as much as 300 mm over the three month period. The heaviest rainfall occurs during the summer months (JJA) when rainfall amounts can reach 350 mm in June (Fig. 4). Compared to observations, on average, the downscaling procedure reasonably captures the seasonal variability of rainfall. Although measurements exhibit greater variability and include extreme events, on a monthly basis the downscaled averaged rainfall reasonably agrees with observations, particularly during the copious precipitation months of the rainy season (JJA). During the later part of the rainy season (OND), rainfall observations tend to be lower than the downscaled quantities (Fig. 4). In terms of the spatial

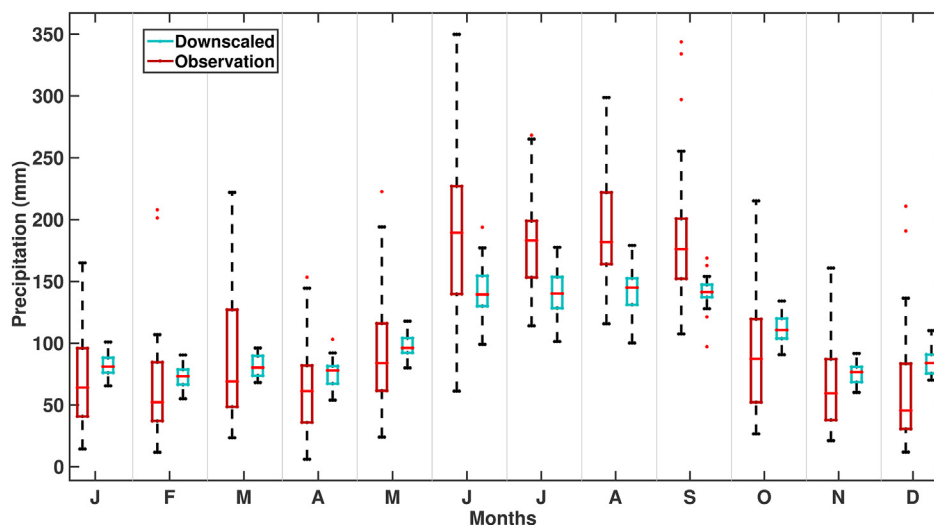


Fig. 4. Comparison of observed and downscaled monthly rainfall averaged for all the stations in the study during the historical period of 1976–2005. For each month, the box plots provide the 10, 25, 50, 75, and 90 percentiles of the rainfall amounts.

distribution of rainfall, the eastern region of south Florida experiences the most abundant rainfall as a result of local sea-breeze-like atmospheric circulation patterns (Cespedes, 2012; Misra et al., 2011). Rainfall is relatively spatially homogeneous during the peak of the rainy season due to the dominance of large-scale atmospheric features such as easterly waves and fronts (Blanchard and Lopez, 1985) that drive convection and formation of precipitating storms (Fig. 5).

The climatological mean precipitation (mm) for each season as obtained from both observations and downscaled GCMs is shown (Fig. 5) for the historical 1976–2005 period. The downscaled and actual observed mean precipitation compare favorably for the MAM and SON seasons, while the downscaling underestimates summer (JJA) mean precipitation and overestimates winter (DJF) mean precipitation over much of the domain (in the latter case, particularly over the southern edge of Florida).

Comparison of the NCEP-downscaled results based on pattern correlation coefficient and root mean square error (RMSE) (see Supplemental material) indicate favorable agreement between NCEP-downscaled and observed precipitation totals. The pattern correlation (Supplementary Fig. 1) yields values close to or exceeding $r = 0.8$ for all seasons.

3.2. Validation of GCM downscaled rainfall during the historical period

By contrast with the high correlation patterns exhibited between observations and NCEP-downscaled historical precipitation, the pattern correlations between observations and raw GCMs results (composite of all 19 GCMs) are generally low at 0.27, -0.02, 0.74, and 0.56 for MAM, JJA, SON, and DJF seasons, respectively. This indicates that the downscaling technique is capable of closely reproducing the actual spatial distribution of rainfall, while the raw GCM average fails to do so, particularly for the spring (MAM) and summer (JJA) seasons. The lack of skill in the raw GCM for JJA puts into question the use of the GCM for JJA that contributes much (roughly 41%) of the total annual rainfall in south Florida (based on the monthly mean precipitation data from 1895 to 2016 provided by National Climatic Data Center; <https://climatecenter.fsu.edu/products-services/data/statewide-averages/precipitation>).

We further investigated the performance of the downscaling approach by analyzing the probability distribution (PDF) of precipitation rate (mm per day) obtained from observations, downscaling of GCMs, and raw GCM precipitation for the historical period, using the 19 observation stations in south Florida (Supplementary Fig. 2). In this process, for the wet-season period only, we categorize precipitation rate from 0.25 to 50.25 mm per day with an interval of 1 mm. Rainfall with >50.25 mm per day is included in the same category with 50.25 mm per day because such a precipitation rate can be considered as heavy rainfall events. In previous studies (Hershfield, 1971; Gallus and Segal, 2004; Ning et al., 2012a), precipitation >0.25 mm per day is considered a wet day or a “rainy day”. We confine our analysis to rainy days.

We find that the downscaled precipitation probability distribution generally resembles the observed precipitation probability distribution, with the notable exceptions of “trace” precipitation events (when precipitation is <1 mm per day). The raw GCM precipitation probabilities, by contrast, are too high compared to observations for “low” precipitation events (precipitation <10 mm per day) and too low for the heavy rainfall category. There is an overall indication of a dry bias in the GCMs, while the downscaled GCM precipitation closely replicates the observations. The downscaling approach shows a marked improvement in all categories of precipitation intensity except the 10–20 mm “moderate rainfall” category. Our finding, that downscaling of the GCMs yields significantly more accurate reproduction of observed precipitation than the raw GCM output, is supported by previous work (e.g., Ning et al., 2012a) reaching the same conclusion for an entirely different (Pennsylvania) region of the U.S.

3.3. Projected changes in precipitation

Having established the improved estimates of downscaled GCM precipitation over the historical era, we next applied the downscaling approach to CMIP5 future projections to yield projections of future seasonal rainfall characteristics in south Florida. We examine climate scenarios corresponding to near (from 2021 to 2050) and far future (from 2071 to 2100) periods. We first consider the middle-ground emissions scenario of RCP4.5 (Fig. 6). Compared to the baseline historical period, we find that mean precipitation is projected to decrease in

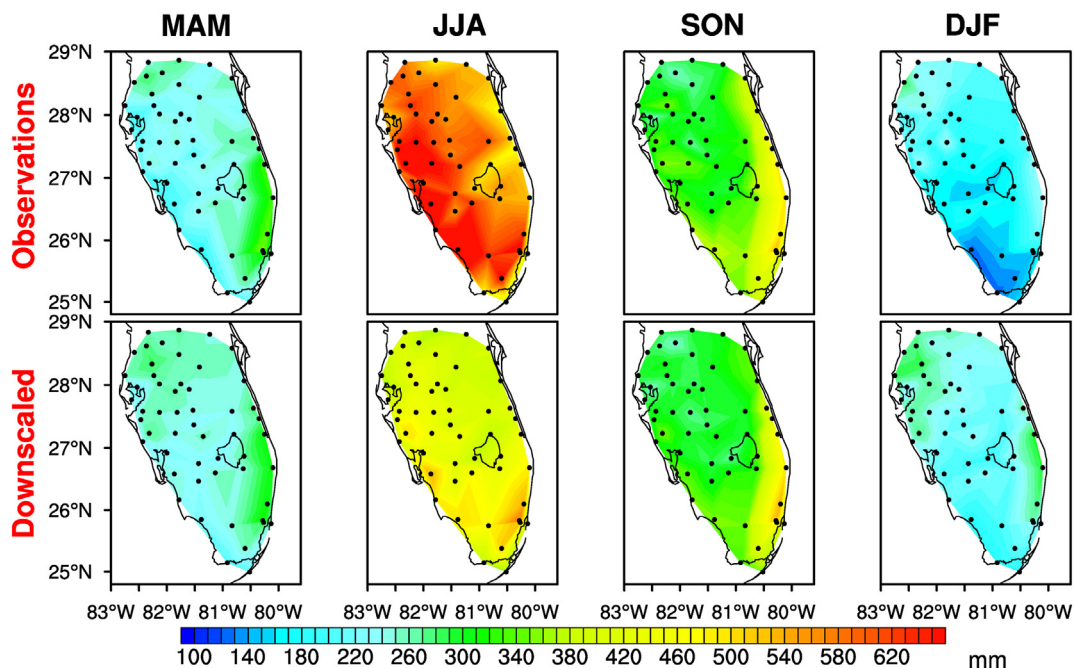


Fig. 5. Seasonal climatological mean precipitation (mm) for MAM, JJA, SON, and DJF seasons during the 1976–2005 historical interval. The upper panel displays results using precipitation observations while the lower panel indicates results from down scaling.

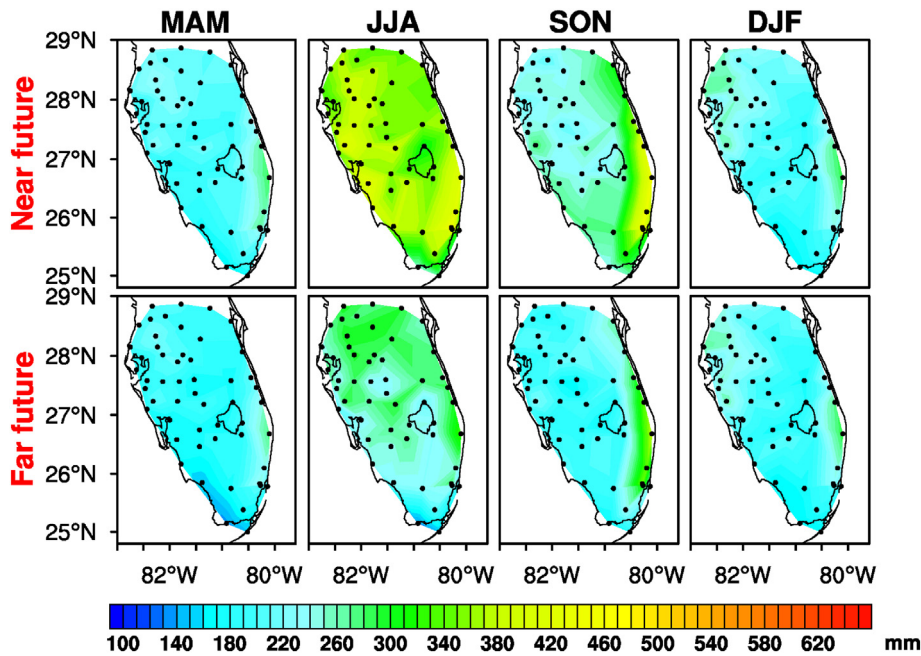


Fig. 6. Seasonal precipitation climatology (mm) computed for MAM, JJA, SON and DJF seasons and shown in upper panel for near future period and in lower panel for far future period using central (RCP4.5) scenario downscaled (constructed final product) data.

the near future and these decreases become more substantial in the far future. Qualitatively similar conclusions are reached for the more aggressive mitigation (RCP2.6) and less aggressive mitigation (RCP8.5) scenarios (results not shown) with the changes being more modest in the former case and more pronounced in the latter case. Some recent studies (Devaraju et al., 2015) argue that climate forcing by large-scale deforestation could play an important role in changing precipitation patterns, leading to further decreases in rainfall totals. We do not account for such impacts in this study.

Fig. 7 shows the uncertainty associated with the precipitation climatology obtained from the downscaled data for the near future RCP4.5

scenario. We consider the realizations that reflect 25% and 75% percentiles in the PDF of grand ensembles (28,500 realizations) to represent the likely climatological precipitation that may occur with minimum (lower bound) and maximum (upper bound) magnitude, respectively. The lower bound shows the least precipitation amount that is most likely to occur for the region, while the upper bound indicates a likely the maximum magnitude of precipitation. It is noticed that the uncertainty has a mostly linear relationship to precipitation climatology. However, there exist considerable spatial variations.

Fig. 8 represents the lower and the upper bound precipitation climatology for far future periods. Fig. 8 suggests that the minimum

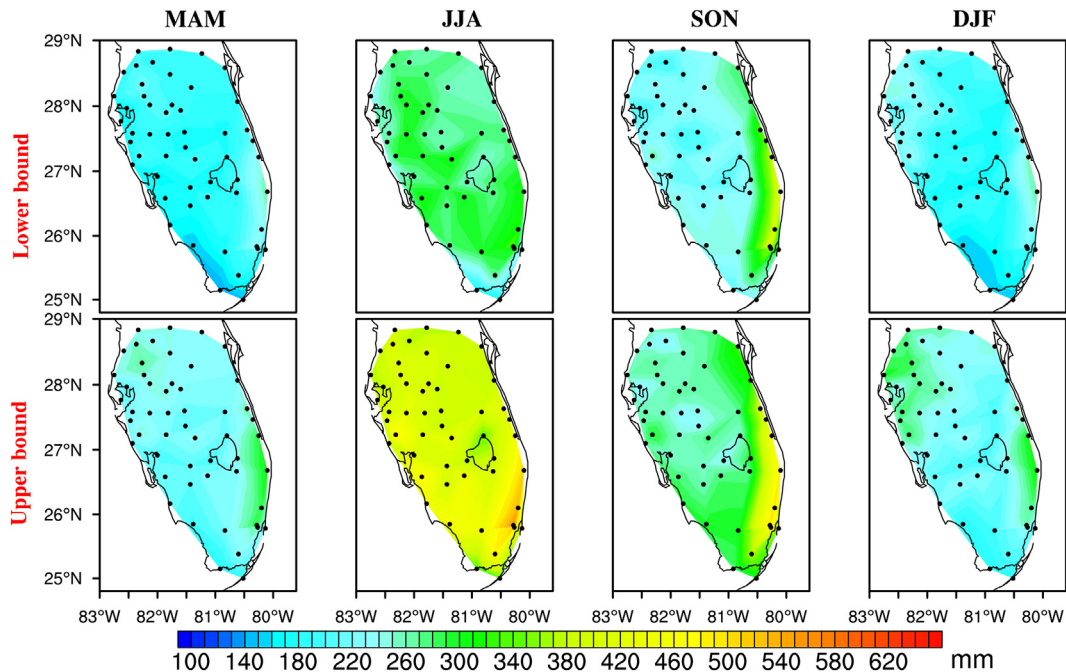


Fig. 7. Uncertainty range for seasonal mean precipitation (mm) computed for the MAM, JJA, SON and DJF seasons and shown in the upper panel for lower bound or minimum and in lower panel for upper bound or maximum precipitation using the central (RCP4.5) scenario downscaled (constructed final product) data for near future scenario.

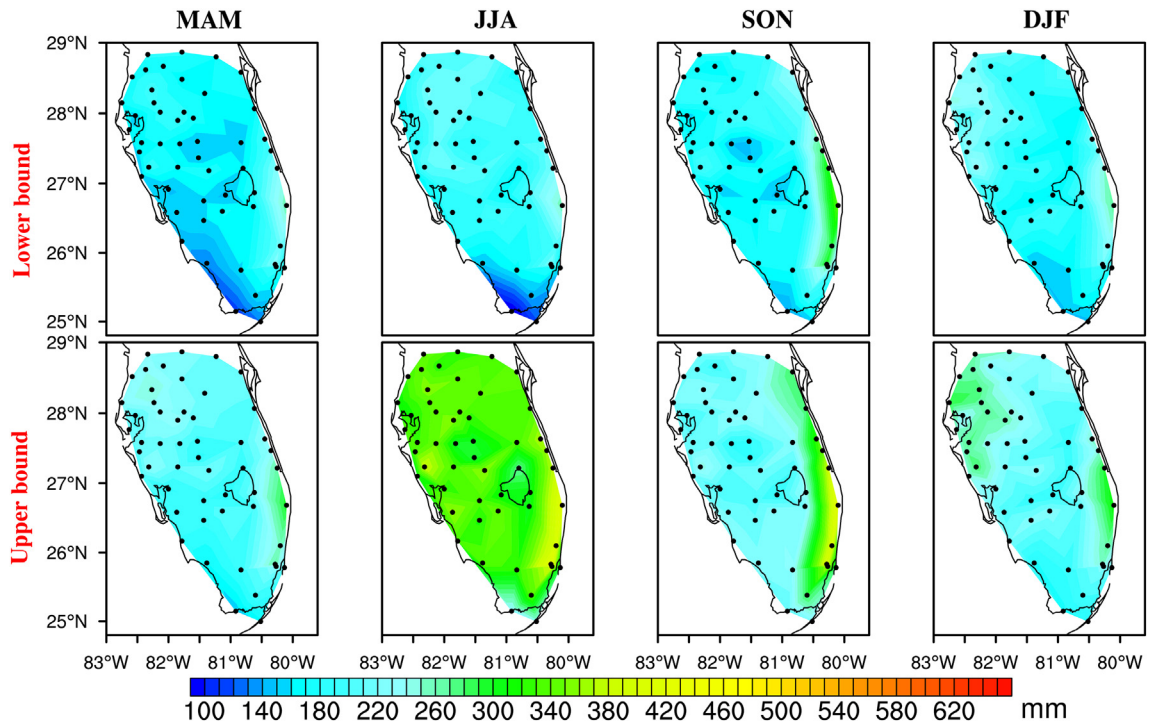


Fig. 8. Uncertainty range for seasonal mean precipitation (mm) computed for the MAM, JJA, SON and DJF seasons and shown in the upper panel for lower bound or minimum and in lower panel for the upper bound or maximum precipitation using the central (RCP4.5) scenario downscaled (constructed final product) data for far future scenario.

precipitation climatology may likely decrease in the far future. The precipitation in the far future is less than the historical period even when the upper bound precipitation is considered. Similar inferences can be made for precipitation climatology and associated uncertainty obtained from the downscaled final product with the use of Method B (Supplementary Figs. 5–7). The reduction in wet season (i.e., in JJA) is notably less during the projected climatic conditions, which could have important consequences to the regional water management systems. We

examined the variability in the GCMs' raw precipitation (based on the spread in the GCMs precipitation) for future periods (Figure not shown) and found that the magnitude and spatial variation in the precipitation uncertainty are higher in the raw GCMs than the downscaled data. This result demonstrates that the downscaling procedure reduces the uncertainty in the projected precipitation changes. Kent et al. (2015) suggested that the regional precipitation changes in the global models are mainly because of shifting patterns in regional convection

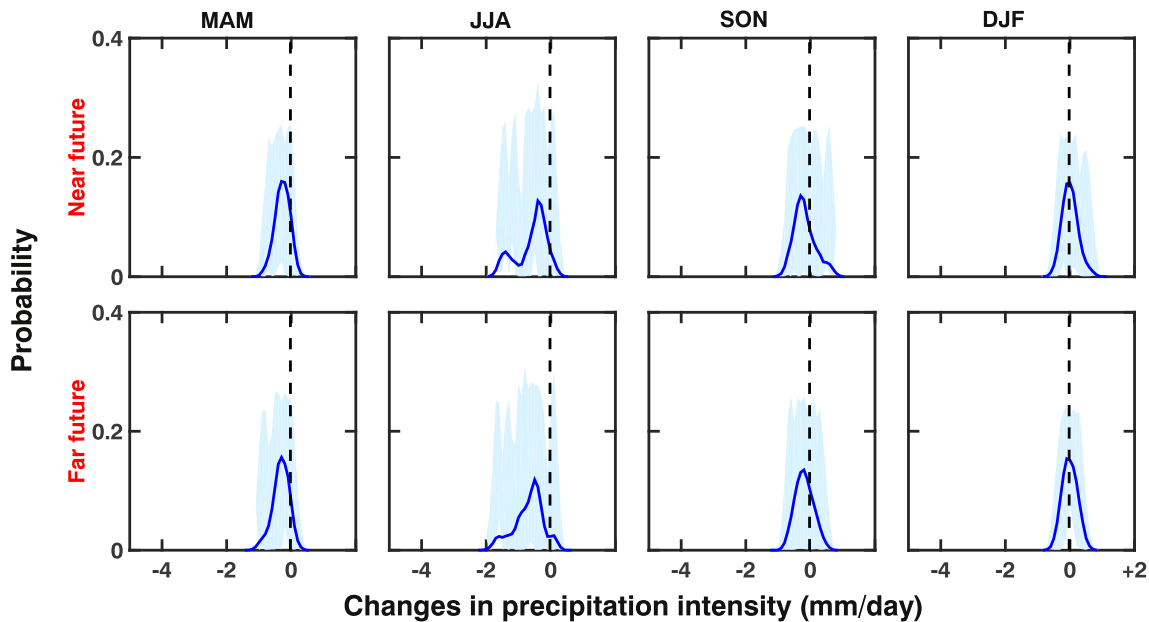


Fig. 9. Probability of projected changes in seasonal precipitation climatology (mm per day) computed for the MAM, JJA, SON and DJF seasons and shown in the upper panel for near future period and in lower panel for far future period using downscaled data. The changes (blue line) in the future are based on downscaled data for historical period and computed using 28,500 iterations of GCMs downscaled data for each period. The spread in the grand ensemble is shown in shaded region. The plot is for the Mountain Lake station (station number 41 in Fig. 1) located north of the south Florida region and for the RCP2.6 scenario. (For interpretation of the references to color in this figure legend, the reader is referred to the web version of this article.)

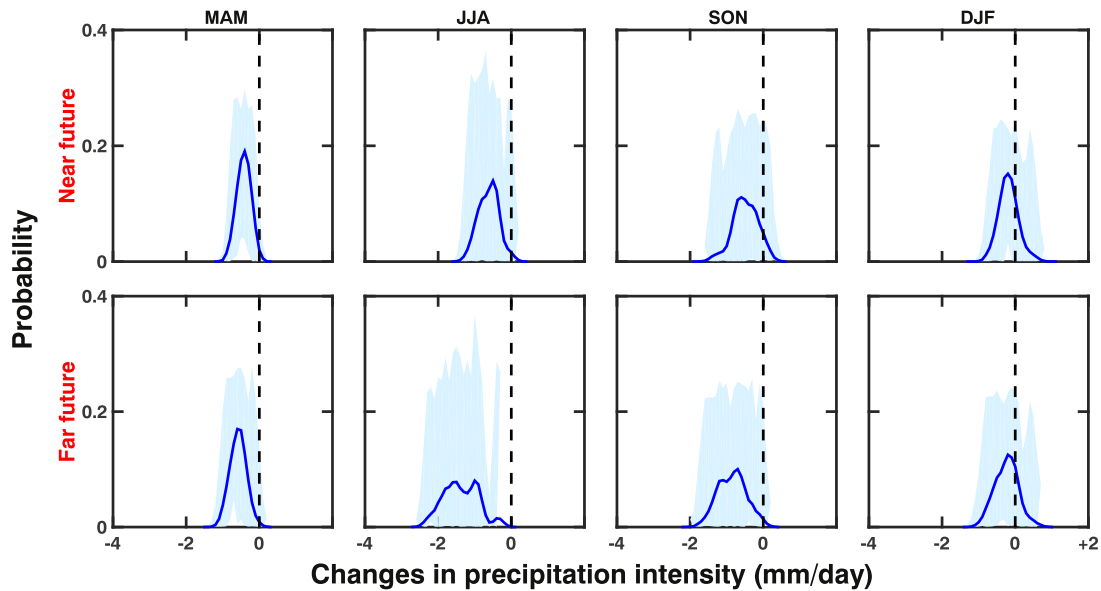


Fig. 10. Same as Fig. 7, but for the RCP4.5 scenario.

and convergence zones. Long et al. (2016) found that the inter-model uncertainty arises due to the different state in the model generated atmospheric circulations. Therefore, taking into account the above fact, the downscaling approach takes multi-model atmospheric circulations as inputs and generates precipitation having less noise. In general, outputs from CMIP5 models indicate drier conditions, particularly during the wet season (June to August) over the southern parts of south Florida (Fig. 8). However, the shift towards drying is small and the uncertainty is higher in the CMIP5 models.

We further examine the “shift” in the precipitation climatology for each station under the influence of each scenario. Fig. 9 shows the probability of projected changes in seasonal precipitation as compared to the historical for the Mountain Lake station (Table 1) and for the RCP2.6 scenario. The shift of the peak in the PDF from “zero” indicates the likelihood in experiencing precipitation changes during the future periods. Interestingly, the PDF curves almost follow the normal distribution. The precipitation climatology for MAM, JJA, and SON seasons will likely

“shift” towards “drier” climate, while DJF precipitation climatology will probably remain unchanged during the future periods. Results (Fig. 8) indicate that the “shift” in the far future is greater than the one for the near future period, suggesting “drier” conditions. The spread in the grand ensembles is narrower during MAM, SON, and DJF seasons, indicating that the uncertainty associated with the precipitation changes is less in the downscaled data. However, the spread in JJA is wider than in the other seasons. This result may be because during the “wet” season rainfall is associated with the complex interactions between small-scale processes (Misra et al., 2011) to the large-scale (Blanchard and Lopez, 1985) convective activity.

Figs. 10 and 11 provide the results of the PDF in precipitation changes for RCP4.5 and RCP8.5 scenarios, respectively. In the near future, for the central scenario, the “shift” increases as compared to the RCP2.6 case. For the Mountain Lake station (Table 1), comparisons of the “shift” for the different scenarios indicate that maximum rainfall changes will likely occur in the RCP8.5 scenario followed by the

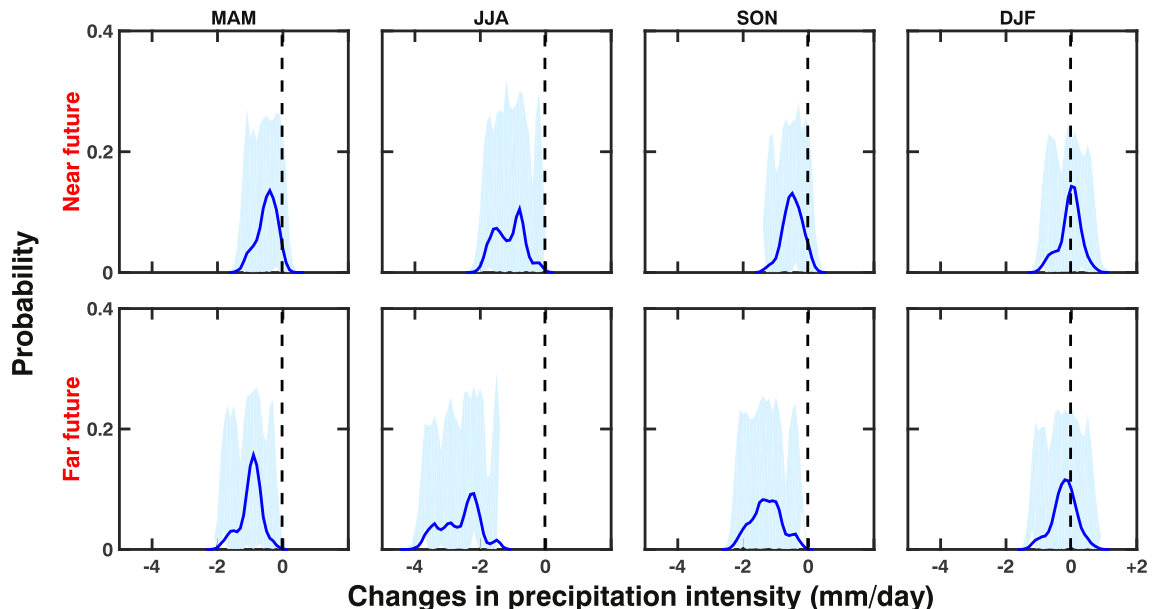


Fig. 11. Same as Fig. 7, but for the RCP8.5 scenario.

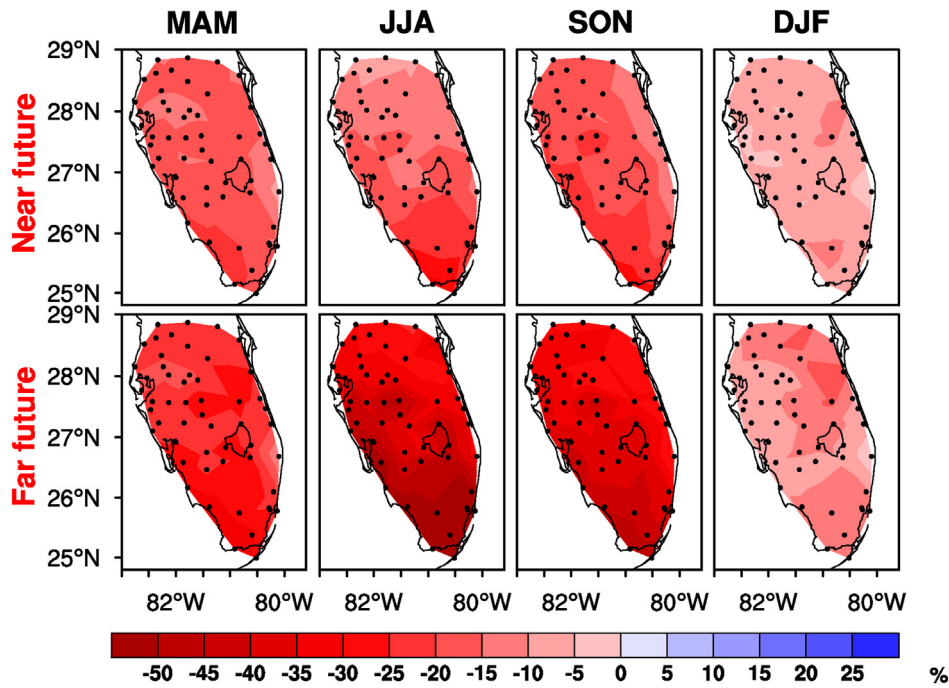


Fig. 12. Changes in seasonal precipitation climatology (in %) during future periods. We use downscaled data for historical and future periods. Computed changes in the future periods are compared to historical (downscaled) data. We use the final product of downscaled from grand ensemble separately for each period and station. The changes in future periods are shown for the central scenario; i.e., for RCP4.5 scenario.

RCP4.5 and RCP2.6 cases in all the seasons except DJF. However, for all the stations, the magnitude of the “shift” is greater in the RCP8.5 and lowest in the RCP2.6 scenarios. It is also noticed that the changes are greater in the far future than the near future. The significance test, using the Mann-Whitney-Wilcoxon technique (Wilcoxon, 1945; Mann and Whitney, 1947) and considering “no changes” in the precipitation climatology as the null hypothesis, reveals that the precipitation changes are significant for 70% (approximately) of the stations for future periods in the case of central scenario. For the RCP8.5 scenario, more stations show significant changes in seasonal precipitation. This result demonstrates that the precipitation changes may occur in the

future climate, and the magnitude of the changes depends on the increases in the trajectory of greenhouse gas loadings.

Comparisons between the results for near and far future conditions reveal that the RCP2.6 scenario does not show any reasonably changes in the occurrences of consecutive dry days. However, the RCP4.5 and RCP8.5 scenarios exhibit notable differences in the consecutive dry days in the far future as compared to near future periods. The rate of changes in the dry episodes is more in the RCP8.5 than the RCP4.5 scenarios. Increases in prolonged dry days will likely cause an increase in the frequency of drought events. The decrease in rainfall will likely enhance the probability of drier climate in the south Florida region.

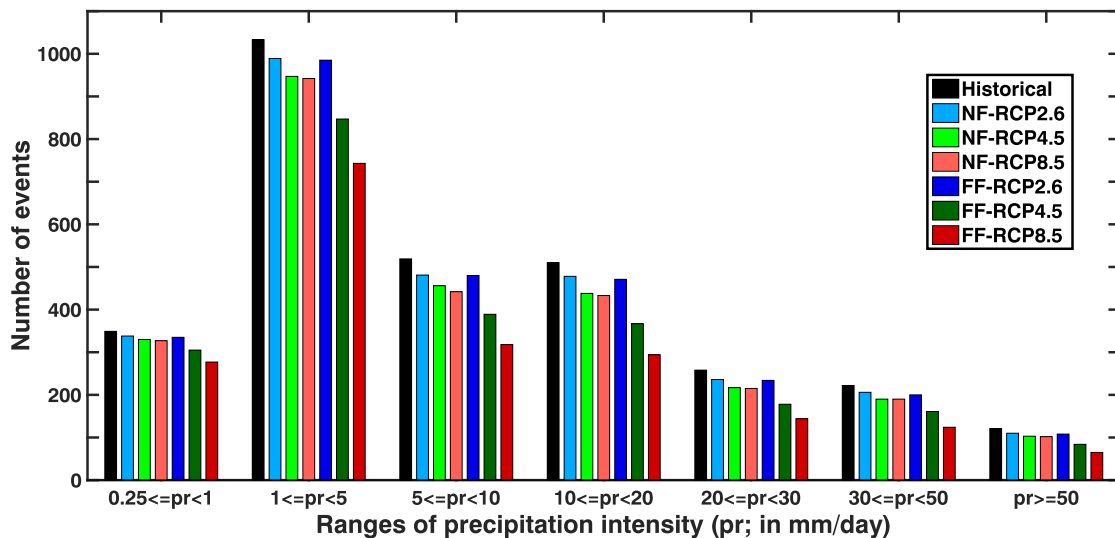


Fig. 13. Total number of wet days (rainfall ≥ 1 mm per day) with different categories of precipitation intensity (mm per day) using GCM downscaled (final product) data for historical (black), near future (light color) and far future (dark color). Near and far future periods for RCP2.6 scenario are represented by light and dark blue, for RCP4.5 scenario are represented by light and dark green and for RCP8.5 scenario are represented by light and dark red colors. We average the wet-events over all the sixty-five stations and use the downscaled data for each period. (For interpretation of the references to color in this figure legend, the reader is referred to the web version of this article.)

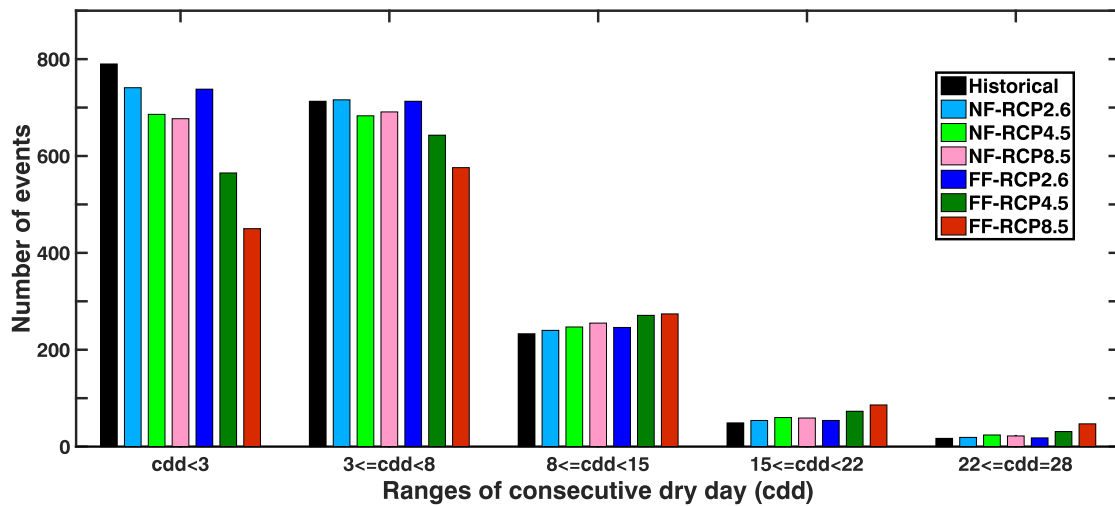


Fig. 14. Same as Fig. 12, but computed for different ranges of consecutive dry day (cdd) events.

Departures of anticipated rainfall amounts are estimated to determine the magnitude of the changes and the impacted areas. For the RCP4.5 scenario, comparisons of results for future periods with the historical record illustrate that the rainfall departures will most likely reach values ranging from 5% to 20% declines over much of south Florida, except during the JJA and SON seasons when far future periods could experience decreased in precipitation exceeding 20% (Fig. 12). On average, compared to the historical period, precipitation will likely decrease by as much as 10 to 15% in the near and far future periods, respectively. Based on the Method B (representative realization is close to observation in terms of climatological values), rainfall departures seem similar (Supplementary Fig. 8) during the future periods, except for DJF season where Method B shows a small increase over some places in south Florida. In the peninsular region of Florida, the extreme projected declines in precipitation reach 50% during the JJA season for the 2071–2100 period under the influence of the RCP4.5 scenario (Fig. 12). The overall expected changes in precipitation using both methods yield almost the same results but rainfall departures exhibit greater uncertainties in the projected precipitation 2071–2100 period. While the exact magnitude of rainfall departures may themselves be uncertain, the consistent patterns of decreased rainfall are significant for future water availability.

It is anticipated that future climatic conditions could influence the frequency of rainfall events in south Florida. To determine the likely rainy events, we consider seven categories of rainfall events based on different ranges of precipitation intensity starting from 0.25 mm per day (Fig. 13). Precipitation is <1 mm per day and more than equal to 1 mm per day is considered as category 1 and intensity >50 mm per day is considered as category 7. Wet days for all categories are likely to decrease in the future periods as compared to the historical record for all the climate scenarios. The rate of decrease in the number of wet days is more in the RCP8.5 scenario. It is noticed in the RCP2.6 scenario that the number of wet days is almost the same in both near and far future periods. In the near future period, the changes in wet days for RCP4.5 and RCP8.5 scenarios are almost the same. In the far future, the decreasing rate is higher with the increasing of RCP scenario from 2.6 to 8.5 $W m^{-2}$.

The number of consecutive dry days (CDD) is also expected to change in south Florida in response to future climate conditions. We investigate the frequency of consecutive dry days in the future periods. Several different categories of consecutive dry days are estimated for historical and future periods (Fig. 14). The number of events is likely to decrease for CDD categories that range from one day to a week. Categories having CDD ranges from 8 to 14 days (~2 weeks range), from 15 to 21 days (~3 weeks range), and from 22 to 28 days (~4 weeks range)

are likely to increase for all the climate scenarios. This result (Fig. 13) is an important finding as prolonged dry episodes may reduce the ground water levels which in turn enhance the possibility of a drought situation.

4. Conclusions

We find that rainfall totals in south Florida downscaled using modern reanalysis of data closely reproduce the observed rainfall totals during the modern historical period (1976–2005). We also found that raw GCM data poorly replicate historical rainfall totals but statistical downscaling of the GCMs more accurately reproduces the historical rainfall totals. Having validated the downscaling approach during the historical era, we applied it to future climate projections. The resulting projections yield an overall drying in all seasons over all of south Florida, the magnitude of which depends on the timeframe (near future versus far future) and the future greenhouse gas emission scenarios. Accordingly, the frequency of wet days decreases and the average length of dry spell increases. The inter-annual variation in projected rainfall is lower in the downscaled data compared to observations, but it is better than the GCM raw outputs. Downscaling methods still need further development to more realistically capture the daily and the inter-annual variability in rainfall patterns observed in south Florida.

Acknowledgements

This material is based upon work supported by the National Science Foundation under Grant number 1204666. The Program for Climate Model Diagnosis and Inter-comparison (PCMDI) and Earth System Grid Federation (ESGF) provided the Climate Model Inter-comparison Project, Phase 5 (CMIP5) data sets. The National Climate Data Center (NCDC) provided the instrumental data sets. Reanalysis derived data were obtained from the National Centers for Environment Prediction (NCEP). Authors thank Tibebe Dessalegne from South Florida Water Management District (SFWMD) for preparing and making available Fig. 4.

Appendix A. Supplementary data

Supplementary data to this article can be found online at <https://doi.org/10.1016/j.scitotenv.2018.04.144>.

References

- Blanchard, D.O., Lopez, R.E., 1985. Spatial patterns of convection in south Florida. *Mon. Weather Rev.* 113 (8), 1282–1299.

- Brekke, L., Dettinger, M., Maurer, E., Anderson, M., 2008. Significance of model credibility in estimating climate projection distributions for regional hydroclimatological risk assessments. *Clim. Chang.* 89, 371–394.
- Cavazos, T., 1997. Downscaling large-scale circulation to local winter rainfall in north-eastern Mexico. *Int. J. Climatol.* 17, 1069–1082.
- Cespedes, R.V., 2012. Florida Rainfall Climatology in Observations and Climate Model Simulations. Thesis Report. University of Miami, pp. 7–11.
- Christensen, J.H., Hewitson, B., Busiuc, A., Chen, A., Gao, X., Held, I., Jones, R., Koli, R.K., Kwon, W.-T., Laprise, R., Rueda, V.M., Mearns, L., Menéndez, C.G., Räisänen, J., Rinke, A., Sarr, A., Whetton, P., 2007. Regional climate projections. In: Solomon, S., Qin, D., Manning, M., Chen, Z., Marquis, M., Averyt, K.B., Tignor, M., Miller, H.L. (Eds.), *Climate Change 2007: The Physical Science Basis*. Contribution of Working Group I to the Fourth Assessment Report of the Intergovernmental Panel on Climate Change. Cambridge University Press, Cambridge, pp. 847–940.
- Clarke, L., Edmonds, J., Jacoby, H., Pitcher, H., Reilly, J., Richels, R., 2007a. Scenarios of greenhouse gas emissions and atmospheric concentrations. Sub-report 2.1A of Synthesis and Assessment Product 2.1 by the U.S. Climate Change Science Program and the Subcommittee on Global Change Research. Department of Energy, Office of Biological and Environmental Research, Washington, D.C., U.S. (154 pp).
- Clarke, L.E., Edmonds, J.A., Jacoby, H.D., Pitcher, H., Reilly, J.M., Richels, R., 2007b. Scenarios of greenhouse gas emissions and atmospheric concentrations. Sub-report 2.1a of Synthesis and Assessment Product 2.1. Climate Change Science Program and the Subcommittee on Global Change Research, Washington, D.C.
- Crane, R.G., Hewitson, B.C., 1998. Doubled CO₂ precipitation changes for the Susquehanna Basin: down-scaling from the genesis general circulation model. *Int. J. Climatol.* 18, 65–76.
- Crane, R.G., Hewitson, B.C., 2003. Clustering and upscaling of station precipitation records to regional patterns using self-organizing maps (SOMs). *Clim. Res.* 25 (2), 95–107.
- Crane, R.G., Yarnal, B., Barron, E.J., Hewitson, B., 2002. Scale interactions and regional climate: examples from the Susquehanna River Basin. *Hum. Ecol. Risk Assess.* 8, 147–158.
- Devaraju, N., Govindasamy, B., Modak, A., 2015. Effects of large-scale deforestation on precipitation in the monsoon regions: remote versus local effects. *Proc. Natl. Acad. Sci.* 112, 3257–3262.
- Flato, G., Marotzke, J., Abiodun, B., Braconnot, P., Chou, S.C., Collins, W., Cox, P., Driouech, F., Emori, S., Eyring, V., Forest, C., Gleckler, P., Guilyardi, E., Jakob, C., Kattsov, V., Reason, C., Rummukainen, M., 2013. Evaluation of climate models. In: Stocker, T.F., Qin, D., Plattner, G.-K., Tignor, M., Allen, S.K., Boschung, J., Nauels, A., Xia, Y., Bex, V., Midgley, P.M. (Eds.), *Climate Change 2013: The Physical Science Basis*. Contribution of Working Group I to the Fifth Assessment Report of the Intergovernmental Panel on Climate Change. Cambridge University Press, Cambridge, United Kingdom and New York, NY, U.S.
- Gallus, W.A., Segal, M., 2004. Does increased predicted warm season rainfall indicate enhanced likelihood of rain occurrence? *Weather Forecast.* 19, 1127–1135.
- Goly, A., Teegavarapu, R.S.V., 2013. Assessment of various statistical downscaling methods for downscaling precipitation in Florida. *World Environmental and Water Resources Congress 2013: Showcasing the Future*, pp. 1086–1098.
- Goyal, M.R., Ojha, C.S.P., 2010. Evaluation of various linear regression methods for downscaling of mean monthly precipitation in arid Pichola watershed. *Nat. Res.* 1, 11–18.
- Harrington, J., Walton, T.L., 2007. *Climate Change in Coastal Areas in Florida: Sea Level Rise Estimation and Economic Analysis to Year 2080*. Center for Economic Forecasting and Analysis. Florida State University, Tallahassee, FL (87p).
- Hartmann, D.L., Klein Tank, A.M.G., Rusticucci, M., Alexander, L.V., Brönnimann, S., Charabi, Y., Dentener, F.J., Dlugokencky, E.J., Easterling, D.R., Kaplan, A., Soden, B.J., Thorne, P.W., Wild, M., Zhai, P.M., 2013. Observations: atmosphere and surface. In: Stocker, T.F., Qin, D., Plattner, G.-K., Tignor, M., Allen, S.K., Boschung, J., Nauels, A., Xia, Y., Bex, V., Midgley, P.M. (Eds.), *Climate Change 2013: The Physical Science Basis*. Contribution of Working Group I to the Fifth Assessment Report of the Intergovernmental Panel on Climate Change. Cambridge University Press, Cambridge, United Kingdom and New York, NY, U.S.
- Hershfield, D.M., 1971. The frequency of dry periods in Maryland. *Chesap. Sci.* 12, 72–84.
- Hewitson, B.C., Crane, R.G., 1992. Large-scale atmospheric control on local precipitation in tropical Mexico. *Geophys. Res. Lett.* 19, 1835–1838.
- Hewitson, B.C., Crane, R.G., 1996. Climate downscaling: techniques and application. *Clim. Res.* 7, 85–95.
- Hewitson, B.C., Crane, R.G., 2006. Consensus between GCM climate change projections with empirical downscaling: precipitation downscaling over South Africa. *Int. J. Climatol.* 26, 1315–1337.
- Kalnay, E., Kanamitsu, M., Kistler, R., Collins, W., Deaven, D., Gandin, L., Iredell, M., Saha, S., White, G., Woollen, J., Zhu, Y., Leetmaa, A., Reynolds, B., Chelliah, M., Ebisuzaki, W., Higgins, W., Janowiak, J., Mo, K.C., Ropelewski, C., Wang, J., Jenne, R., Joseph, D., 1996. The NCEP/NCAR 40-year reanalysis project. *Bull. Am. Meteorol. Soc.* 77, 437–471.
- Kent, C., Chadwick, R., Rowell, D.P., 2015. Understanding uncertainties in future projections of seasonal tropical precipitation. *J. Clim.* 28, 4390–4413.
- Khan, M.S., Coulibaly, P., Dibikey, Y., 2006. Uncertainty analysis of statistical downscaling methods. *J. Hydrol.* 319, 357–382.
- Kohonen, T., 1989. *Self-Organization and Associative Memory*. 3rd ed. Springer-Verlag (312 pp).
- Kohonen, T., 1995. *Self-Organization Maps*. Springer, Berlin (362pp).
- Kosovich, J.J., 2008. State of Florida 1:24,000- and 1:100,000-scale quadrangle index map—highlighting low-lying areas derived from USGS digital elevation models: U.S. Geological Survey Scientific Investigations Map 3047, scale 1:1,000,000.
- Krause, P., Boyle, D.P., Base, F., 2005. Comparison of different efficiency criteria for hydrological model assessment. *Adv. Geosci.* 5, 89–97.
- Kumar, S., Merwade, V., Kinter, J.L., Niyogi, D., 2013. Evaluation of temperature and precipitation trends and long-term persistence in CMIP5 twentieth-century climate simulations. *J. Clim.* 26, 4168–4185.
- Long, S., Xie, S., Liu, W., 2016. Uncertainty in tropical rainfall projections: Atmospheric circulation effect and the ocean coupling. *J. Climate* 29:2671–2687. <https://doi.org/10.1175/JCLI-D-15-0601.1>.
- Mann, H.B., Whitney, D.R., 1947. On a test of whether one of two random variables is stochastically larger than the other. *Ann. Math. Stat.* 18 (1), 50–60.
- Maraun, D., Wetterhall, F., Ireson, A.M., Chandler, R.E., Kendon, E.J., Widmann, M., Brienen, S., Rust, H.W., Sauter, T., Themeßl, M., Venema, V.K.C., 2010. Precipitation downscaling under climate change: recent developments to bridge the gap between dynamical models and the end user. *Rev. Geophys.* 48 (3).
- Misra, V., Moeller, L., Stefanova, L., Chan, S., O'Brien, J.J., Smith, T.J., Plant, N., 2011. The influence of the Atlantic warm pool on the Florida panhandle sea breeze. *J. Geophys. Res.-Atmos.* 116 (D21), 1–14.
- Moss, R.H., et al., 2010. The next generation of scenarios for climate change research and assessment. *Nature* 463, 747–756.
- Murphy, J., 1999. An evaluation of statistical and dynamical techniques for downscaling local climate. *J. Clim.* 12, 2256–2284.
- Ning, L., Mann, M.E., Crane, R., Wagener, T., 2012a. Probabilistic projections of climate change for the mid-Atlantic region of the United States: validation of precipitation downscaling during the historical era. *J. Clim.* 25, 509–526.
- Ning, L., Mann, M., Crane, R., Wagener, T., Najjar, R., Singh, R., 2012b. Probabilistic projections of anthropogenic climate change impacts on precipitation for the mid-Atlantic region of United States. *J. Clim.* 25, 5273–5291.
- Obeysekera, J., Irizarry, M., Park, J., Barnes, J., Dessalegn, T., 2011. Climate change and its implications for water resources management in south Florida. *Stoch. Env. Res. Risk A.* 25, 495–516.
- Portmann, R.W., Solomon, S., Hegerl, G.C., 2009. Spatial and seasonal patterns in climate change, temperatures, and precipitation across the United States. *Proc. Natl. Acad. Sci.* 106, 7324–7329.
- Rayer, S., Wang, Y., 2017. Projections of Florida Population by County, 2020–2045, with Estimates for 2016. Vol. 50. Bureau of Economic and Business Research, University of Florida (Bulletin 177). https://www.bebr.ufl.edu/sites/default/files/Research%20Reports/projections_2017.pdf.
- Rhein, M., Rintoul, S.R., Aoki, S., Campos, E., Chambers, D., Feely, R.A., Gulev, S., Johnson, G.C., Josey, S.A., Kostianoy, A., Mauritzen, C., Roemmich, D., Talley, L.D., Wang, F., 2013. Observations: ocean. In: Stocker, T.F., Qin, D., Plattner, G.-K., Tignor, M., Allen, S.K., Boschung, J., Nauels, A., Xia, Y., Bex, V., Midgley, P.M. (Eds.), *Climate Change 2013: The Physical Science Basis*. Contribution of Working Group I to the Fifth Assessment Report of the Intergovernmental Panel on Climate Change. Cambridge University Press, Cambridge, United Kingdom and New York, NY, U.S.
- Rousi, E., Anagnostopoulou, C., Tolika, K., Maheras, P., 2015. Representing teleconnection patterns over Europe: a comparison of SOM and PCA methods. *Atmos. Res.* 152, 123–137.
- Sarojini, B.B., Stott, P.A., Black, E., Polson, D., 2012. Fingerprints of changes in annual and seasonal precipitation from CMIP5 models over land and ocean. *Geophys. Res. Lett.* 39, L21706. <https://doi.org/10.1029/2012GL053373>.
- Schoof, J.T., Pryor, S.C., 2001. Downscaling temperature and precipitation: a comparison of regression-based methods and artificial neural networks. *Int. J. Climatol.* 21, 773–790.
- Schoof, J.T., Shin, D.W., Cocke, S., LaRou, T.E., Limb, Y.-K., O'Brien, J.J., 2009. Dynamically and statistically downscaled seasonal temperature and precipitation hindcast ensembles for the southeastern USA. *Int. J. Climatol.* 29, 243–257.
- Sinha, P., Mohanty, U.C., Kar, S.C., Dash, S.K., Robertson, A., Tippett, M., 2013. Seasonal prediction of the Indian summer monsoon rainfall using canonical correlation analysis of the NCMRWF global model products. *Int. J. Climatol.* 33:1601–1614. <https://doi.org/10.1002/joc.3536>.
- Smith, S.K., Rayer, S., 2013. Projections of Florida population by county, 2015–2040, with Estimates for 2012. Vol. 46. Bureau of Economic and Business Research (Bulletin 165, March 2013).
- Snell, S.E., Gopal, S., Kaufmann, R.K., 2000. Spatial interpolation of surface air temperatures using artificial neural networks: evaluating their use for downscaling GCMs. *J. Clim.* 13, 886–895.
- Swain, E., Stefanova, L., Smith, T., 2014. Applying downscaled global climate model data to a hydrodynamic surface-water and groundwater model. *Am. J. Clim. Chang.* 3, 33–49.
- Taylor, K.E., Stouffer, R.J., Meehl, G.A., 2011. An overview of CMIP5 and the experiment design. *Bull. Am. Meteorol. Soc.* 93, 485–498.
- Trimble, P., Obeysekera, J., Cadavid, L., Santee, E., 2005. Application of climate outlooks for water management in south Florida. *Climate Variations, Climate Change, and Water Resources Engineering*: pp. 65–85 <https://doi.org/10.1061/9780784408247.ch05>.
- Tripathi, S., Srinivas, V.V., Nanjundiah, R.S., 2006. Downscaling of precipitation for climate change scenarios: a support vector machine approach. *J. Hydrol.* 330, 621–640.
- Wagener, T., Sivapalan, M., Troch, P.A., McGlynn, B.L., Harman, C.J., Gupta, H.V., Kumar, P., Rao, P.S.C., Basu, N.B., Wilson, J.S., 2010. The future of hydrology: an evolving science for a changing world. *Water Resour. Res.* 46, W05301. <https://doi.org/10.1029/2009WR008906>.
- Wilby, R.L., Wigley, T.M.L., 1997. Downscaling general circulation model output: a review of methods and limitations. *Prog. Phys. Geogr.* 21, 530–548.
- Wilby, R.L., Wigley, T.M.L., Conway, D., Jones, P.D., Hewitson, B.C., Main, J., Wilks, D.S., 1998. Statistical downscaling of general circulation model output: a comparison of methods. *Water Resour. Res.* 34, 2995–3008.
- Wilcoxon, F., 1945. Individual comparisons by ranking methods. *Biom. Bull.* 1 (6), 80–83.
- Wilks, D.S., 1995. *Statistical Methods in the Atmospheric Sciences*. 2nd ed. vol. 59. Academic Press, San Diego, p. 464.
- Wood, A.W., Leung, L.R., Sridhar, V., Lettenmaier, D.P., 2004. Hydrologic implications of dynamical and statistical approaches to downscaling climate model outputs. *Clim. Chang.* 62, 189–216.